DTIC FILE COPY

(2)

SECURITY CLASSIFICATION OF THIS PAGE

REPORT DOCUMENTATION PAGE

Form Approved OMB No. 0704-0188

1a. REPORT SECURITY CLASSIFICATION UNCLASSIFIED	1b. RESTRICTIVE MARKINGS
AD-A217 878	3. DISTRIBUTION/AVAILABILITY OF REPORT Approved for public release; distribution unlimited.
DTIC ELECTE FEB 07 1990 D	5. MONITORING ORGANIZATION REPORT NUMBER(S) AFOSR-TR- 90-0088

6a. NAME OF PERFORMING ORGANIZATION UNIVERSITY OF HOUSTON	6b. OFFICE SYMBOL (If applicable)	7a. NAME OF MONITORING ORGANIZATION AIRFORCE OFFICE OF SCIENTIFIC RESEARCH
6c. ADDRESS (City, State, and ZIP Code) 4800 CALHOUN BLVD. DEPT. OF MECH. ENGR. HOUSTON, TX 77204-4792		7b. ADDRESS (City, State, and ZIP Code) AFOSR/NA Bolling AFB DC 20332-6448 BOLLING AFB, DC 30332
8a. NAME OF FUNDING/SPONSORING ORGANIZATION AFOSR	8b. OFFICE SYMBOL (If applicable) NA	9. PROCUREMENT INSTRUMENT IDENTIFICATION NUMBER AFOSR-87-0183
8c. ADDRESS (City, State, and ZIP Code) AFOSR/NA Bolling AFB DC 20332-6448		10. SOURCE OF FUNDING NUMBERS

PROGRAM ELEMENT NO.	PROJECT NO.	TASK NO.	WORK UNIT ACCESSION NO.
61102F	2302	B2	

11. TITLE (Include Security Classification)
STRESS FIELD NEAR CRACK TIP: AN EXPERIMENTAL EVALUATION OF THE THREE DIMENSIONAL VARIATION (U)

12. PERSONAL AUTHOR(S)
K. RAVI-CHANDAR

13a. TYPE OF REPORT	13b. TIME COVERED	14. DATE OF REPORT (Year, Month, Day)	15. PAGE COUNT
FINAL	FROM 5/1/87 TO 8/31/89	1989/11/30	34

16. SUPPLEMENTARY NOTATION

17. COSATI CODES			18. SUBJECT TERMS (Continue on reverse if necessary and identify by block number)
FIELD	GROUP	SUB-GROUP	FRACTURE, SCATTERED LIGHT PHOTOELASTICITY, THREE DIMENSIONAL PROBLEMS

19. ABSTRACT (Continue on reverse if necessary and identify by block number)

This report summarizes the results on the project obtained during the two year period. A new special purpose laboratory equipment called the Scattered Light Polariscope has been designed and constructed. The Polariscope system consists of a device for loading the specimen, optical alignment devices for precise positioning of the specimen with respect to the incident light and an imaging system with a video camera, digitizing frame grabber and image processing software. The systems have all been assembled and tested for proper operation. Certain limitations of the current photoelastic equations were performed. Calibration experiments have been performed to determine the reliability of the technique as well as the data interpretation procedures. Results have been obtained on the nature of the stress variation near the tip of a rounded notch and a crack. Significant differences have been demonstrated between the two and three dimensional stress fields. KEYWORDS!

20. DISTRIBUTION/AVAILABILITY OF ABSTRACT ☒ UNCLASSIFIED/UNLIMITED ☐ SAME AS RPT. ☐ DTIC USERS	21. ABSTRACT SECURITY CLASSIFICATION UNCLASSIFIED
22a. NAME OF RESPONSIBLE INDIVIDUAL GEORGE K. HARITOS, LTCOL	22b. TELEPHONE (Include Area Code) (202) 767-0463 / 22c. OFFICE SYMBOL

DD Form 1473, JUN 86 Previous editions are obsolete.

SECURITY CLASSIFICATION OF THIS PAGE
UNCLASSIFIED

18 DEC 1989

Final Technical Report to

The Air Force Office of Scientific Research

STRESS FIELD NEAR A CRACK TIP:

AN EXPERIMENTAL EVALUATION OF THE

THREE DIMENSIONAL VARIATION

K. Ravi-Chandar

NOVEMBER 1989

GRANT NUMBER-87-0183

UH

DEPARTMENT OF MECHANICAL ENGINEERING
UNIVERSITY OF HOUSTON
HOUSTON, TX 77204-4792

Abstract

This report summarizes the results on the project obtained during the two year period. A new special purpose laboratory equipment called the Scattered Light Polariscope has been designed and constructed. The Polariscope system consists of a device for loading the specimen, optical alignment devices for precise positioning of the specimen with respect to the incident light and an imaging system with a video camera, digitizing frame grabber and image processing software. The systems have all been assembled and tested for proper operation. Certain limitations of the current photoelastic equations were determined and therefore a complete reexamination of the photoelastic equations was performed. Calibration experiments have been performed to determine the reliability of the technique as well as the data interpretation procedures. Results have been obtained on the nature of the stress variation near the tip of a rounded notch and a crack. Significant differences have been demonstrated between the two and three dimensional stress fields.

INTRODUCTION

The stress field near the tip of a through crack in a plate of finite thickness is known to have a three dimensional character. However, due to the analytical complexity of the problem, two dimensional approximations of plane stress or plane strain are usually introduced in interpreting the crack tip stress state. Under the two dimensional approximation, the stress field near the crack tip is completely determined by a single parameter K_I, called the stress intensity factor. The fracture toughness of a material is then that value of K_I at which crack growth initiates, denoted by K_{IC}. However, crack growth does not occur uniformly through the plate thickness and hence the two-dimensional approach represents an idealization of the actual situation. Also, the critical stress intensity factor at initiation seems to be dependent on the plate thickness.

An attempt was made by Roaskis and Ravi-Chandar (1984) to determine experimentally, the range of validity of the two dimensional approximations. Using the experimental method of caustics, measurements were made at different distances from the crack tip and compared with two dimensional analyses. It was found that a state of plane stress was established only at distances of about one half of the plate thickness away from the crack tip. Furthermore, no significant region where a plane strain field dominated was found. Some of these conclusions have also been obtained analytically by Yang and Freund (1985). The main upshot of these results is that the plane asymptotic singular field characterized by the stress intensity factor K_I does not determine the conditions local to the crack tip where the fracture processes occur. It is still true, however, that K_I remains a useful measure of the energy available for the fracture process as along as a strain energy density function is used to characterize the material behavior.

Analyses of the linear elastic problem using the full three dimensional theory of elasticity have been presented by Folias (1975) for a plate of finite thickness and by Bentham (1977) for a quarter-infinite crack in a half-space. However, these solutions have not been used much in fracture mechanics, probably due to the difficulties in interpretation. Smith and co-workers (1975,1983, and 1984), have used frozen stress photoelasticity to investigate the three dimensional problems. While much of their early work concentrated on three dimensional crack geometries such as the part through and corner cracks, recently, they have addressed inherently three dimensional problems in finite thickness plates. Their experimental results support the analysis of Bentham by indicating that the inverse square root singularity of the two dimensional analysis is lost near the faces of the plate. The technique of frozen stress photoelasticity involves machining

of the specimens into thin slices after stress freezing and then examining the slices using two dimensional or transmitted light photoelasticity. In the present investigation, scattered light photoelasticity has been used. This is a non-invasive, non-destructive technique, and in the present investigation, some fundamental improvements have been made in both the interpretation of the data and the implementation of the experimental scheme. These are outlined in detail in the following sections.

II. THE THEORY OF PHOTOELASTICITY

In 1939, Weller made a remarkable discovery: the light field scattered by a transparent elastic material subjected to a stress field exhibited fringes that could be related to the stresses. He published this information as a half page letter to the editor! Drucker and Mindlin (1940) developed the corresponding theory to analyse the fringe patterns and extract the stress variation. Weller (1941) implemented the technique of scattered light photoelasticity and published pictures of fringes that were of astounding quality; very few pictures of similar quality appear in later literature. Since this early development, a number of authors, notably, Jessop (1951), Frocht and Srinath (1958), Srinath and Frocht (1962), Cheng(1969), and Srinath(1983), have explored the technique further both in theoretical development and experimental implementation. However, the technique has remained esoteric, not only because of specialized equipment and interpretation needed to obtain information, but also because the sensitivity (stress fringe value) was quite low. In the following, we propose a novel implementation of the technique of scattered light photoelasticity that enhances the sensitivity considerably. In fact, a fringe pattern is already established in the specimen and applied stresses only cause changes in this fringe pattern, thus making the technique similar to mismatch moire, for example. We briefly review some aspects of crystal optics in Section II.1 The stress optic law and its tensorial character are discussed in detail in Section II.2. The principles of scattered light photoelasticity and its interpretation are outlined in Section II.3. An example applied to the proposed model material, Homalite-100 is given; it is demonstrated that this material is an optical uniaxial crystal. Finally in Section II.4, the new model material is used to examine the classical disk problem to illustrate the application and then the notch and crack problems are considered.

II.1 Some Aspects Of Crystal Optics

Crystalline media exhibit optical anisotropy; i.e., the speed of propagation of light depends on the direction of propagation and the plane of polarization. It can be shown that, (see Coker and Filon (1957), Born and Wolf (1965)) for any given direction of propagation, two polarizations of the electric vector characterizing the electromagnetic wave are possible and in general the speeds of the two components are different. This fact forms the basis of all photoelastic techniques. We shall briefly review the effects of optical anisotropy resulting from electrical anisotropy in crystalline materials. Magnetic anisotropy and its effect on optical anisotropy are small in most materials and therefore is not considered here. The magnetic permeability will be considered to be unity.

Electrical anisotropy may be represented through the relationship between the electric field vector, **E**, and electric displacement vector, **D**, as follows[1]:

$$D_i = \varepsilon_{ij} E_j \tag{1}$$

where ε_{ij} are the components of the dielectric tensor. The inverse relation can be written as

$$E_i = a_{ij} D_j \tag{2}$$

where a_{ij} are the components of the the tensor **a**, which is the inverse of ε. The refractive index can be denoted by a tensor **n** given by $\sqrt{\mathbf{a}}$. The "square-root" of a symmetric tensor of order two is uniquely defined when in the common principal frame, the components of **n** are taken as the square root of the principal values of **a** {see Stephenson (1980)}. In general, the electric displacement is not in the same direction as the electric field. In such anisotropic media, is possible to propagate "two monochromatic plane waves, with two different linear polarizations and two different velocities"[2] in any given direction. Furthermore, the components of the dielectric tensor may be represented graphically as an ellipsoid

$$\varepsilon_{ij} x_i x_j = 0 \tag{3}$$

This is referred to as the *ray ellipsoid or Fresnel ellipsoid.* A similar representation can be provided for the components of the tensor **a**; the corresponding ellipsoid is called the *index ellipsoid or the ellipsoid of wave normals.* In light of the new definition of the refractive index as a tensor square root of **a**, a **refractive index ellipsoid** could also be constructed. The Fresnel and the index ellipsoids provide a graphical means of determining the refractive indices for rays propagating in arbitrary directions. Consider a ray propagating in the direction[3] **s** as indicated in

[1] Latin subscripts admit the range 1,2,3; Greek subscripts admit the range 1,2. Summation convention is used.

[2] Born and Wolf (1965), p.671.

Figure 1, where a Fresnel ellipsoid is also illustrated. The intersection of the plane normal to s with the ellipsoid is an ellipse; let the directions of the major and minor axes of this ellipse, which will be referred to as the *secondary principal directions*, be denoted by x'_α. The two plane polarized waves that can be propagated lie along the secondary principal directions. The speeds of propagation for the two different polarizations are given by the semi-major and semi-minor axes of the ellipse. The refractive index is given directly by the secondary principal values of the refractive index tensor **n**.

Since ε is symmetric, there exists a principal frame in which the components of ε can be represented in diagonal form. Let ε_i be the principal values of ε. If all the principal values are equal, then $\varepsilon_{ij} = \varepsilon\delta_{ij}$, $a_{ij} = a\delta_{ij}$,where $\varepsilon=1/a$ and ε and a are constant. Then the electric field and displacement are in the same direction and the medium is optically isotropic; the corresponding Fresnel ellipsoid collapses to a sphere. If two principal values are equal, then isotropy is lost; the corresponding Fresnel and index ellipsoids are ellipsoids of revolution. Thus, the direction corresponding to the unique principal value is fixed while the other two principal directions may be chosen arbitrarily in the plane perpendicular to the unique principal direction. This unique principal direction is called the *optic axis*; such a medium is referred to as a *uniaxial crystal*. We shall show later that in photoelastic applications, an initially isotropic medium becomes a uniaxial crystalline medium. If all three principal values are distinct, then there are no symmetries associated with the Fresnel ellipsoid. However, it can be shown that there exist two distinct axes normal to which the ellipsoid is sectioned into circles. These two axes are the optical axes for this medium and materials which exhibit this behavior are referred to as *biaxial crystals*.

Some polymeric materials that are optically isotropic, become anisotropic upon an imposed stress or deformation. If the deformation is reversible, the anisotropy disappears on the removal of the load; on the other hand, if large irreversible deformations are imposed, the anisotropy becomes permanent. In other polymers, during the casting or molding process, a permanent molecular orientation is introduced which results in optical anisotropy. This temporarily or permanently induced anisotropy can be used to determine the stress and deformation in such materials or the molecular orientation and the residual stress field and this idea forms the basis of photoelasticity. In the following section, we describe the *stress optic law* that is based on Wertheim's model.

[3] The ray direction will always be denoted by s.

II.2. Stress-Optic Law

In this section, we derive the forms of the stress optic law commonly used in photoelasticity in such a way that it can be applied to transmitted as well as scattered light photoelasticity. Viewing the photoelastic medium as an optical medium that may be initially optically isotropic or anisotropic and which becomes weakly optically anisotropic upon the application of load, photoelasticity is described in the setting of crystal optics discussed above. This is essential since in our implementation of scattered light photoelasticity, we use an uniaxial optical crystal as the model material.

Consider a light ray propagating along a direction **s** as indicated in Figure 1, entering the photoelastic medium subjected to a stress field $\sigma(\mathbf{x})$. Under conditions of small deformations, it may be assumed that the changes in the dielectric tensor or the index tensor are a linear function of the stress state or deformation. The coefficients in this relationship are referred to as the *stress-optical* or *piezo-optical coefficients*. This linear relationship, suggested by Wertheim(1854), Maxwell(1852) and Neumann (1841) can be written in a generalized form as follows:

$$a_{ij}(\mathbf{x}) - a_{ij}^{0} = \chi_{ijkl}\sigma_{kl}(\mathbf{x}) \tag{4}$$

where χ is a constant tensor of fourth order called the *stress-optic tensor* with symmetries somewhat similar to the elasticity tensor **C** relating the stress and strain tensors. The symmetry of **a** and σ impose certain symmetries on χ, reducing the number of constants in the most general case to 36. Bhagavantham (1942, 1952) has investigated the effect of various crystal symmetries on the tensor χ. We will look at only the special case of isotropic photoelastic symmetry in the photoelastic effect; i.e., χ is isotropic. The medium, however, may be initially optically anisotropic or isotropic, and the applied stress $\sigma(\mathbf{x})$ may also be anisotropic, resulting in optical anisotropy in the stressed medium. Given that the changes in the tensor **a** under the applied stress is small, Eq.(4) may be replaced with a corresponding expression for the refractive index tensor:

$$n_{ij}(\mathbf{x}) - n^{0}_{ij} = \psi_{ijkl}\sigma_{kl}(\mathbf{x}) \tag{5}$$

In fact, since experiments only measure the optical path difference which is proportional to the difference in refractive index, the above equation represents a more convenient form of the stress optic law.

II.2.1 Isotropic Photoelastic Effect: For a photoelastically isotropic medium, i.e., the stress optic effect is independent of direction of propagation of light, only two components of χ are unique and

can be represented as

$$\chi_{ijkl} = \alpha\delta_{ij}\delta_{kl} + \beta(\delta_{ik}\delta_{jl} + \delta_{il}\delta_{jk}) \tag{6}$$

where α and β are the only stress optic coefficients needed to define the photoelastic effect. Substituting the above into Eq.(4), yields:

$$a_{ij}(\mathbf{x}) - a^0_{ij} = \alpha\sigma_{kk}(\mathbf{x})\delta_{ij} + \beta\sigma_{ij}(\mathbf{x}) \tag{7}$$

This relationship is similar in form to the linear elastic relationship between the components of the strain tensor and the components of the stress tensor. The form of this equation indicates that α determines the hydrostatic contribution while β provides the contribution of the (deviatoric) shear stresses.

Initially isotropic medium with isotropic photoelastic effect: From Eq.(7), it is clear that the principal axes of the stress tensor and the principal axes of the refractive index tensor in the stressed medium coincide *if and only if the medium is initially isotropic*; i.e., $a^0_{ij} = a^0\,\delta_{ij}$. Then the above relationship reduces to the standard form of the stress optic law when expressed in this common principal frame.

$$\begin{aligned} a_1(\mathbf{x}) - a^0 &= (\alpha+\beta)\sigma_1(\mathbf{x}) + \alpha[\sigma_2(\mathbf{x}) + \sigma_3(\mathbf{x})] \\ a_2(\mathbf{x}) - a^0 &= (\alpha+\beta)\sigma_2(\mathbf{x}) + \alpha[\sigma_3(\mathbf{x}) + \sigma_1(\mathbf{x})] \\ a_3(\mathbf{x}) - a^0 &= (\alpha+\beta)\sigma_3(\mathbf{x}) + \alpha[\sigma_1(\mathbf{x}) + \sigma_2(\mathbf{x})] \end{aligned} \tag{8}$$

where $(\alpha + 2\beta)$ and α are called the *direct and transverse stress optic coefficients* respectively. For the ray propagating in an arbitrary direction **s**, the incident polarized ray is decomposed into two components and propagated with different velocities. The appropriate refractive indices can be obtained through the graphical construction outlined earlier. Consider a right handed coordinate system given by (s, x'_1 and x'_2) as indicated in Figure 1, where x'_1 and x'_2 are chosen such that they are along the semi-major and semi-minor axes of the ellipse given by the intersection of the plane normal to s with the Fresnel ellipsoid. Only light rays whose **D** vectors are aligned along x'_1 and x'_2 can propagate along the s direction. The corresponding components of **a** in the frame (s, x'_1 and x'_2) are a'_{11} and a'_{22}; by the special choice of the coordinate frame, $a'_{12} = 0$. The components of the stress tensor $\sigma(\mathbf{x})$ in this frame are denoted by σ'_{11}, σ'_{22}, σ'_{ss}, σ'_{2s} and σ'_{s1}; once again, $\sigma'_{12} = 0$ due to the choice of coordinates. The components σ'_{11}, σ'_{22}, and σ'_{ss} are referred to as the *secondary principal stresses* and are the only components that influence the changes in the refractive index[4]. The stress optic law can then be written in in terms of the

secondary principal stresses:

$$\begin{aligned} a'_{11}(x') - a^0 &= (\alpha + \beta)\sigma'_{11}(x') + \alpha[\sigma'_{22}(x') + \sigma'_{ss}(x')] \\ a'_{22}(x') - a^0 &= (\alpha + \beta)\sigma'_{22}(x') + \alpha[\sigma'_{11}(x') + \sigma'_{ss}(x')] \end{aligned} \tag{9}$$

Thus, for an arbitrary direction of propagation, s, two component rays with polarizations along the directions x'_1 and x'_2 are propagated. The refractive indices for these two component rays are given by $n'_1 = 1/\sqrt{a'_{11}}$ and $n'_2 = 1/\sqrt{a'_{22}}$. Thus, the two rays accumulate a phase difference as the ray propagates through the medium. The relative difference is given by

$$a'_{11}(x') - a'_{22}(x') = \beta\,[\sigma'_{11}(x') - \sigma'_{22}(x')] \tag{10}$$

Note that the relative difference is independent of the hydrostatic component of stress. Thus, by measurements of the relative changes, the full stress field cannot be determined. However, if the absolute changes in the refractive index are measured, this limitation of photoelasticity may be overcome. In terms of the refractive index, Eq.(10) can be written as

$$n'_1(x') - n'_2(x') = C\,[\sigma'_{11}(x') - \sigma'_{22}(x')] \tag{11}$$

where $n'_1(x')$ and $n'_2(x')$ are the refractive indices for the two polarizations that can propagate along s. In terms of optical path difference, the "relative retardation," $\Delta(\mathbf{x})$, can be written as:

$$\Delta(x) = \frac{2\pi}{\lambda}\int_0^{\mathbf{x}} [n'_1(x') - n'_2(x')]ds = \frac{2\pi}{\lambda}\int_0^{\mathbf{x}} C[\sigma'_{11}(x') - \sigma'_{22}(x')]\, ds \tag{12}$$

where λ is the wavelength of light. It is assumed at this stage that the secondary principal directions do not change along the path of the ray, although this assumption can be relaxed with considerably more effort. The key idea in photoelasticity is to combine the two components and extract the phase difference for determination of the secondary principal stresses. This can be done in two ways: first, the after the two components exit the photoelastic medium they are combined by passing through a polarizing filter, resulting in constructive or destructive interference depending

[4] If the stress state at the point of entry is described by the Lame stress ellipsoid, $\sigma_{ij}x_ix_j = 0$, then the intersection of the Lame ellipsoid with the plane normal to s describes an ellipse. The semi-major and semi-minor axes of this ellipse are referred to as the secondary principal axes, denoted by x'_α and the stress components along these directions are referred to as the *secondary principal stresses* (*effective stresses* in the terminology of Weller), denoted by σ'_α. These definitions are similar to the definition of the secondary principal refractive indices and the corresponding axes. If the standard Wertheim's law of temporary double refraction (isotropic photoelastic effect) is used, then the ellipsoid of refractive index is aligned parallel to the Lame ellipsoid of stress. Since the refractive indices for a ray propagating in the x_3 direction is given by the semi-major and semi-minor axes of the ellipse given by the intersection of the index ellipsoid with the plane $x_3 = 0$ (see Born and Wolf (1965), p.674), the refractive indices for rays polarized along the secondary principal stress axes are a linear function of the secondary principal stresses σ'_α.

on the phase difference. This is the standard application of transmitted light photoelasticity. The resulting fringe patterns can only provide information the integral of the secondary principal stresses along the ray path.

$$\bar{\sigma}'_{11} - \bar{\sigma}'_{22} = \frac{f_\sigma}{2\pi h}\Delta(x_1,x_2) = \frac{f_\sigma}{h}N(x_1,x_2) \tag{13}$$

where $\bar{\sigma}'_{11}$, $\bar{\sigma}'_{22}$ are averaged over the path of the light beam. In the second implementation, the two components are made to scatter from the specimen in a direction normal to s. This scattering may be achieved either by molecular scattering or by introducing secondary particles in the model material that enhances scattering. Upon scattering, the two components are plane polarized in the x'_1-x'_2 plane and combine to provide interference fringes. Since scattering can occur from arbitrary points in the specimen, the thickness variation of the stress components can be extracted from the gradient of the fringe variation:

$$\sigma'_{11}(x') - \sigma'_{22}(x') = f_\sigma \frac{\partial N(x')}{\partial s} = \frac{f_\sigma}{2\pi h}\frac{\partial \Delta(x')}{\partial s} \tag{14}$$

Thus, through the scattered light implementation of photoelasticity, it is possible to obtain the spatial variation of $\sigma'_{11}(x')$ - $\sigma'_{22}(x')$ without thickness averaging.

Note that as outlined here, the only difference between scattered light photoelasticity and transmitted light photoelasticity occurs in the way in which the two polarized components are recombined to provide information on the path difference $\Delta(x')$. In the scattered light technique, the specimen itself acts as the 'analyser' used in transmitted light photoelasticity, permitting evaluation of $\Delta(x')$ even in the interior of the specimen.

Initially anisotropic medium with isotropic photoelastic effect: Now let us consider a medium for which $a^0_{ij} \neq a^o \delta_{ij}$. Then the principal axes of the Lame ellipsoid and the Fresnel ellipsoid do not coincide! Eqs. (4) cannot be simplified further. However, if we consider the light propagation direction s to lie completely in a plane of symmetry of the specimen, then one principal direction must lie along s, implying that σ'_{2s} and σ'_{s1} are zero. σ'_{11}, σ'_{22}, σ'_{ss} and σ'_{12} are nonzero. The secondary principal stresses σ'_1, σ'_2, can be obtained from Mohr's transformation as

$$\sigma'_{1,2} = \frac{\sigma'_{11} + \sigma'_{22}}{2} \pm \sqrt{\left(\frac{\sigma'_{11} - \sigma'_{22}}{2}\right)^2 + (\sigma'_{12})^2} \tag{15}$$

and the stress optic law becomes:

$$a'_{11}(x') - a^0_{11} = (\alpha + \beta)\sigma'_1(x') + \alpha[\sigma'_2(x') + \sigma'_s(x')]$$
$$a'_{22}(x') - a^0_{22} = (\alpha + \beta)\sigma'_2(x') + \alpha[\sigma'_1(x') + \sigma'_s(x')] \tag{16}$$

Once again, if only the relative retardation is considered, we get

$$a'_{11}(x') - a'_{22}(x') = \{a'^0_{11} - a'^0_{22}\} + \beta\{\sigma'_1(x') - \sigma'_2(x')\} \tag{17}$$

In terms of the refractive indices, the relative retardation may be written as

$$n'_1(x') - n'_2(x') = \{n'^0_1 - n'^0_2\} + C\{\sigma'_1(x') - \sigma'_2(x')\} \tag{18}$$

Thus the stress-optic law for transmitted and scattered light photoelasticity may be written as:

$$\Delta(x) = \frac{2\pi}{\lambda}\int_0^x [n'_1(x') - n'_2(x')]ds = \frac{2\pi}{\lambda}\{n'^0_1 - n'^0_2\}x + \frac{2\pi}{\lambda}\int_0^x C[\sigma'_{11}(x') - \sigma'_{22}(x')]\, ds \tag{19}$$

For planes other than those of symmetry, Eqs.(4) must be used and detailed measurements of the refractive index have to be made in order to identify the principal axes and thereby identify the stress components. We do not investigate this aspect here, but will address it in a future contribution. We now turn to scattered light photoelasticity and its implementation in an initially anisotropic medium.

III. SCATTERED LIGHT PHOTOELASTICITY: A NOVEL IMPLEMENTATION

The details of the implementation of this technique are available in text books such as those by Dally and Riley (1978) and Kukse and Robertson (1974). A more recent monograph by Srinath (1983) is devoted entirely to scattered light photoelasticity. Therefore, we do not provide an analysis of the light vector as it travels through the specimen; only the results are given. Consider a sheet of light polarized along the direction 1-1 travelling in the direction s as shown in Figure 2. Let the secondary principal direction x'_2 be oriented at an angle θ with respect to the plane of polarization 1-1. If the light scattered from the point Q is viewed along a direction at an angle φ to the secondary principal direction x'_2, then the intensity of the scattered light field may be obtained as:

$$I(x') = K\ \{\cos^2\theta\sin^2\varphi + \sin^2\theta\cos^2\varphi - (1/2)\sin 2\theta \sin 2\varphi \cos\Delta(x')\} \tag{20}$$

where K depends on the incident light amplitude as well as the scattering properties of the medium. It is easily shown that when $\theta = \varphi = \pi/4$, the resulting intensity is given by

$$I(x') = (1/2)K\ (1 - \cos\Delta(x')) \tag{21}$$

Thus, if the secondary principal directions are known (fixed), then the angles φ and θ may be adjusted such that the scattered light field intensity depends only on the secondary principal stresses. The fringes, formed as the loci of the corresponding light intensity points, will be similar to the isochromatics in transmitted light photoelasticity, although the interpretation should the through Eq. (19). On planes of symmetry and on stress free bounding surfaces, the secondary principal directions can easily be established and therefore, we illustrate in the present paper a applications of scattered light photoelasticity under these conditions.

III.1 Scattered Light Polariscope

The conventional transmitted light polariscope is not suitable for the scattered light investigations. Weller (1939) built a rather simple, inexpensive version of the scattered light polariscope, concentrating mainly on the generation of the incident light sheet, with the appropriate plane of polarization. Most polariscopes built later did not use light sheets, but merely light pencils, thereby limiting the available information from any one experiment. Weller also pointed out to the need for immersing the complete specimen, along with any loading frame, in a tank filled with a fluid of matching refractive index, to eliminate refractions at entry into and exit from the specimen. The polariscope built for the present investigation is shown in Figure 3. The main idea used in the design of this polariscope is that the plane of the light sheet remains fixed in space; the plane of polarization, the plane of observation and the orientation of the specimen which is intersected by the light sheet are variable and controlled by precision rotating and translating stages. A 6mW He-Ne Laser is used as the coherent light source which produces a pencil of light rays with a known plane of polarization. The laser beam, initially travelling horizontally, is deflected upwards along the direction **s**, by a mirror. The light beam is then expanded and collimated into a light sheet by a pair of cylindrical lenses. The laser beam can be rotated about the **s** axis, thereby permitting variation of the plane of polarization with respect to the plane of the light sheet. The specimens are loaded in a specially designed loading frame, containing a hermetically sealed load cell, that can be immersed in a tank containing a fluid with a refractive index matching that of the specimen.

III.2 Scattering in Optical Crystals

Consider a light ray propagating along the direction **s** incident on an optically anisotropic medium, linearly polarized at an angle φ with respect to the major principal direction. Upon entering the

medium, the polarized light is decomposed into two components each polarized along the principal directions. Since the speed of propagation of the two components are different, they accumulate a path difference Δ, given by Eq. (19) with $\sigma = 0$. Upon scattering, the intensity is given by

$$I(x') = \frac{1}{2}K\left\{ 1 - \cos\left[\frac{2\pi}{\lambda}(n'^{0}_{1} - n'^{0}_{2})\{s - \xi(x'_1)\} \right]\right\} \tag{22}$$

where $\{s-\xi(x'_1)\} = 0$ represents the equation for the entrance boundary of the specimen in the plane $x'_2 = 0$.. Thus the fringes should be parallel to the boundary of the specimen. Scattering properties of most optical crystals, such as Nicols prism, is very poor and thus, the prediction of Eq. (22) is not easily observed. However, Homalite-100[5], a thermosetting polyester, possesses good molecular scattering properties and is also optically anisotropic. The latter is due to molecular orientation introduced in the casting process. The prediction of Eq.(22) is shown to be correct experimentally, as illustrated in Figure 4, where the scattered light fields due to light incidence on three different planes of a circular disk are shown.

If the scattered light intensity predicted by Eq.(22) is measured, then such measurements can be used to determine the components of the refractive index tensor. This is illustrated below.

III.3 Characterization of Optical Properties of Homalite-100

We now turn to an investigation of the optical anisotropy of Homalite-100, in order to (i) determine the principal refractive indices and (ii) to determine the stress-optic constants through some calibration experiments. Since the specimen material is manufactured in the form of cast sheets, we shall introduce a consistent coordinate notation to keep track of the sheet, the principal refractive axes and the principal stress axes. The direction normal to the sheet of the specimen will be denoted by X_3. The directions in the plane of the specimen will be denoted by X_α and the specific orientation will be dictated by the specimen boundaries in the plane $X_3 = 0$. The principal refractive axes will be denoted by N_i, with the corresponding refractive indices indicated by n_i. The principal stress axes will be denoted by Σ_i and the corresponding stress components denoted by σ_i. The coordinate system specific to the light propagation direction will still be indicated by (s, x'_1 and x'_2) where s is the light propagation direction and x'_1 and x'_2 are the secondary principal directions.

III.3.1. Optical Anisotropy of Homalite-100: Figure 4 shows three photographs of the scattered light field under the following conditions: (i) s direction is aligned parallel to X_1 with the light

[5] Trademark of SGL Homalite, Delaware

sheet in the X_1-X_2 (4a) and X_3-X_1 (4b) planes; (ii) s direction is aligned parallel to X_3 with the light sheet in the X_3-X_1 (4c) plane. First, note that the existence of variations in the intensity of the scattered light field in the different pictures is indicative of the optical anisotropy of Homalite-100. Secondly, when s is in the direction of X_3, uniform scattered light intensity is observed. This implies that the rays with polarizations along the secondary principal directions x'_1 and x'_2 do not experience any path difference; i.e., the secondary principal refractive indices n'_1 and n'_2 are equal. This is possible in a general anisotropic medium (biaxial crystal) only if s were in the direction of the optic axis. Finally, by continuously varying the direction s from the X_3 direction to $-X_3$ direction in the X_2-X_3 plane, no other optic axis was found implying that the specimen was a uniaxial crystal, with the principal refractive index axes N_i aligned along the specimen axes X_i. i.e., the index ellipsoid is an ellipsoid of revolution, with the axis of revolution aligned along X_3 or N_3.

III.3.2. Stress Optic Coefficients of Homalite-100: The stress-optic coefficients were determined through a number of calibration experiments using simple specimen loading conditions where the stress field is completely known from elementary elastic analysis. Planar tensile specimen and a disk with diametral compression were used in the calibration experiments. In both these cases, plane stress conditions may be assumed since the plate thickness was quite small. Thus, the principal stress direction Σ_3 coincides with the direction X_3 of the specimen and also with the principal refractive index direction N_3. Furthermore, the uniaxial crystalline nature of the specimen implies that when a plane stress field is applied, the principal stress axes Σ_1 and Σ_2 should coincide with the principal refractive index axes N_1 and N_2 (planar isotropy). Thus in this instance (and in any case when there is a plane of symmetry that is aligned with a principal refractive index axis) the Lame ellipsoid and the Fresnel ellipsoid are parallel. Two stress-optic constants indicating the changes in n'_1 and n'_2 should completely determine the stress optic effect for s coinciding with X_3. Furthermore, if one is interested only in the relative retardation as in Eq.(19), then only one stress optic coefficient has to be determined.

Consider a bar loaded in tension as indicated in Figure 5. The orientation of the specimen axes, loading direction and the principal refractive axes are also indicated in this figure. The fringes in the unloaded state are parallel to the entry surface and are uniformly spaced. From the fringe spacing, once again $n'_1 - n'_3$ can be determined. Upon applying a uniform tensile stress field, the fringe spacing changes, but still remains straight. From the new fringe spacing, using

Eq.(19), the applied stress σ'_{22} can be obtained, if f_σ is known; otherwise, this experiment is used to calibrate f_σ.

IV. APPLICATIONS OF SCATTERED LIGHT PHOTOELASTICITY

We now turn to some examples to illustrate the capability of the technique of scattered light photoelasticty. Two examples will be illustrated; the first one is the classical problem of a circular disk under diametral compressive loads. It is shown that by observing the scattered light field from three orientations, the stress components $\sigma_{\alpha\beta}$ can be determined. Furthermore, if it is assumed that plane conditions hold, which is reasonable for this geometry, the stress components $\sigma_{\alpha\beta}$ can be obtained directly at all field points with the need for elaborate separation techniques used in transmitted light photoelasticity! The second example concerns a plate with a notch (similar to a compact tension specimen, except that the crack is replaced with a rounded notch). Finally, the stress field near the tip of a crack, and its dependence on the specimen thickness is investigated.

IV.1. Determination of Stress Components from Scattered Light Field

We now turn to the determination of the individual stress components from observations of the scattered light field. Consider a plane of symmetry or the bounding surface of a plate, with some stress distribution. Clearly $\sigma_{3\alpha} = 0$; on the bounding surface, σ_{33} is also zero. If the scattered light from a light sheet lying on this plane is observed, the intensity is given by Eq.(21) where D(x) is given by Eq. (19). The secondary principal stresses will depend on the direction of light propagation s in the X_1 - X_2 plane. Consider three angles of light incidence along $\theta = 0$ and $\theta = \pm\alpha$, as indicated in Figure 6. The corresponding secondary principal stresses are $\sigma_{22} - \sigma_{33}$, $\sigma'_{11} - \sigma_{33}$ and $\sigma''_{11} - \sigma_{33}$. But, σ'_{11} and σ''_{11} are related to through the Mohr transformation equations:

$$\begin{aligned} \sigma'_{11} &= \sigma_{11}\cos^2\alpha + \sigma_{22}\sin^2\alpha + 2\sigma_{12}\sin\alpha\cos\alpha \\ \sigma''_{11} &= \sigma_{11}\cos^2\alpha + \sigma_{22}\sin^2\alpha - 2\sigma_{12}\sin\alpha\cos\alpha \end{aligned} \tag{23}$$

Thus, using Eq.(14), from the measurements, the fringe gradients corresponding to the secondary principal stress differences $\sigma_{22} - \sigma_{33}$, $\sigma'_{11} - \sigma_{33}$ and $\sigma''_{11} - \sigma_{33}$ can be obtained. Let us denote the corresponding fringe gradients as follows:

$$\sigma_{22}(x) - \sigma_{33}(x) = \frac{\partial N(x)}{\partial x_1} - \frac{\partial N_0}{\partial x_1} \equiv G(x)$$

$$\sigma'_{11}(x) - \sigma_{33}(x) = \frac{\partial N'(x)}{\partial x'_1} - \frac{\partial N_0}{\partial x'_1} \equiv G'(x) \tag{24}$$

$$\sigma''_{11}(x) - \sigma_{33}(x) = \frac{\partial N''(x)}{\partial x''_1} - \frac{\partial N_0}{\partial x''_1} \equiv G''(x)$$

Then the stress differences are obtained as:

$$\sigma_{22}(x) - \sigma_{33}(x) = G(x)$$

$$\sigma_{11}(x) - \sigma_{22}(x) = \frac{G'(x) + G''(x) - 2G(x)}{2\cos^2\alpha} \tag{25}$$

$$\sigma_{12}(x) = \frac{G'(x) - G''(x)}{2\sin 2\alpha}$$

once the variation of the fringe gradients at every point is known. If the plane is on a bounding traction free surface, σ_{33} is zero and hence the above equations can be used to determine the *individual stress components directly without the need for elaborate separations techniques* used in transmitted light photoelasticity.

IV.1. Disk under Diametral Compression

As an example of the application of the technique, consider the disk problem illustrated in Figure 7. The unloaded and loaded scattered light fields for once angle of incidence along the line of the load application is shown. If the fringe gradients before and after loading, along the light path, are determined, then, the variation of the stress component can be obtained. Figure 8a shows the fringe spacing data before and after loading, and Figure 8b shows the calculated values of σ_{11}; for comparison, the classical elastic results (Timoshenko and Goodier (1970)) are also shown in this figure. As can be seen, there is good agreement between the theory and experiment. It is possible to determine the stress components at every point completely using this method, but the above suffices to illustrate the point.

IV.2. Notch Specimen

The second example of application concerns a notched specimen shown in Figure 9. Two different specimen thicknesses were considered (9.525mm and 12.7mm). The scattered light field from the

unloaded and loaded specimen are shown in Figure 10, for light incidence along the $-x_1$ direction. From these and two other sets of observations of the scattered light fields corresponding to $\theta = \pm \alpha$, Eq.(25) could be used to determine $\sigma_{11} - \sigma_{22}$ and σ_{12}. The experiment can be repeated for light incidence along both the specimen midplane and the free surfaces. Figure 11 shows the variation of these stress components along the x_1 axis. It is seen that the mid plane stresses are considerably higher than the face plane stresses. In Figure 12, isochromatic contours, corresponding to equal values of $\sigma_{11} - \sigma_{22}$ are shown. Figure 12a shows the contour corresponding to the same stress difference, while Figure 12b shows the two different contours correpsonding to two different values of the stress difference that pass through the same point ahead of the notch tip. Further analysis of the stress fields is possible using the technique illustrated here to determine the details of the three dimensional variation, but this is not attempted here.

IV.3. Compact Tension Specimen

We consider next, a Compact Tension (CT) specimen, in order to investigate the three dimensionality of the crack tip stress field. From the scattered light analysis, the stress component σ_{22} is determined directly at all points on the free surfaces, and $\sigma_{22} - \sigma_{33}$ is determined at all points on the specimen mid-plane. With the observation technique discusses earlier, it is not possible to separate σ_{22} and σ_{33} in the midplane without investigation of the stress field in other planes. The variations of $\sigma_{22} - \sigma_{33}$ on the midplane and σ_{22} on the face plane with distance from the crack tip are shown in Figure 13. In Figure 14, the isochromatics corresponding to $(\sigma_{11} - \sigma_{22})$ from the midplane and face plane are shown for the two specimen thicknesses of 6.35mm and 12.7mm, for the same value of $(\sigma_{11} - \sigma_{22})$. Since the distance at which this ischomatic exists in the thicker specimen is much closer to the crack tip than in the thinner specimen, we see that Figure 13a, corresponding to the 6.35 mm thick specimen shows close agreement with the 2D theory, while te conrours in Figure 13b, corresponding to the 12.7mm thick specimen, exhibits large differences. From an examination of the results in Figures 13 and 14, it is immediately apparent that the midplane stresses are higher than the face plane. Furthermore, at a distance of r/h = 0.5, the mid plane and face plane results appear close to the 2D theory. Thus, the range of validity of the 2D field is definitely at distances greater than r/h =0.5. This reinforces earlier, indirect results of Rosakis and Ravi-Chandar (1986). Moreover, recent numerical computations of Parsons, Hall and Rosakis (1986), indicate that the σ_{22} near the face plane has exactly the same variation shown

in Figure 13b. Their results are reproduced in Figure 15. Figure 15a corresponds to the specimen midplane and Figure 15b shows the radial variation of σ_{22} in the traction free surface. Their results for the midplane are not directly comparable since they plot only the radial variation of σ_{22} and not (σ_{11} - σ_{22}) as we have done in Figure 13a. From the results of Parsons *et al* (1988), σ_{33} is a positive quantity which decays away from the crack tip and goes to zero at about $r/h = 0.5$; also near the crack tip, as once proceeds from the traction free surfaces to the midplane, σ_{33} increases. Therefore, we expect that σ_{22} in the midplane will be larger than the 2D prediction. Further work is under progress to determine the full variation of the stress components in other planes, and will be reported elsewhere.

References

Bentham, J.P., (1977), *Int J Solids and Struct*, **13**, pp.479-492.

Bhagavantham, S., (1942), *Proc Ind Acad Sci A*, **16**.

Bhagavantham, S., (1952), *Acta Crystallogr*, **5**, p.591.

Born, M., and E. Eolf, (1965), Principles of Optics, Pergamon Press, Oxford.

Cheng, Y.F., (1969), *Experimental Mechanics*, **9**, p.407.

Coker, E.G, and L.N.G.Filon, (1957) A Treatise on Photoelasticity, Cambridge University Press.

Dally J.W., and Riley, W.F., (1978), Experimental Stress Analysis, McGraw Hill, New York.

Drucker, D.C., and R.D. Mindlin, (1940), *J Appl Phys*, **11**, pp.724-732.

Folias, E.S., (1975), *J Appl Mech*, **42**, pp.663-674.

Frocht, M.M., and Srinath, L.S., (1958), *Proc 3rd US Nat Cong App Mech*, pp.329-337.

Jessop, H.T., (9151), *Brit J Appl Phys*, **2**, pp.249-260.

Kukse, A., and G. Robertson, (1974), Photoelastic Stress Analysis, John Wiley, London.

Maxwell, C., (1852), *Trans Roy Soc Edin*, vol xx, part I.

Neumann, F.E., (1841), *Abh. d. Kõn Acad d Wissenschaften zu Berlin*, part II, pp.1-254.

Parsons, I.D., J.F. Hall and A.J. Rosakis, (1986) "A finite element investigation of the elastostatic state near a three dimensional edge crack,:GALCIT SM-86-29, California Institute of Technology, Pasadena.

Rosakis, A.J., and K. Ravi-Chandar, (1986), *Int J of Solids and Struct*, **22**, (1986), 121-134.

Smith, C.W., (1975), in Experimental Techniques in Fracture Mechanics, 2, SESA Monograph No. 2., (ed. A.S. Kobayashi), pp.3-58.

Smith, C.W., and J.S. Epstein, (1983), *Proc of the 10th Canadian Fracture Conference*

Smith, C.W., and J.S. Epstein, (1984), *Proc of the Vth Int Cong on Exp Mech.*

Srinath, L.S., and M.M. Frocht, (1962) *Proc 4th US Nat Cong App Mech*, pp.775-781.

Srinath, L.S., (1983), Scattered Light Photoelasticity, Tata McGraw HIll, New Delhi.

Stephenson, R.A., *J Elasticity*, **10**, pp.213-214.

Weller, R., (1939), *J Appl Phys*, **10**, p.266.

Weller, R., (1941), *J Appl Phys*, **12**, pp.610-616.

Wertheim, G., (1854), *Annales de Ch et de Phys*, Ser III, vol XL, p. 156.

Yang W., and Freund, L.B., (1985), *Int J of Solids and Struct*, **21**, p. .

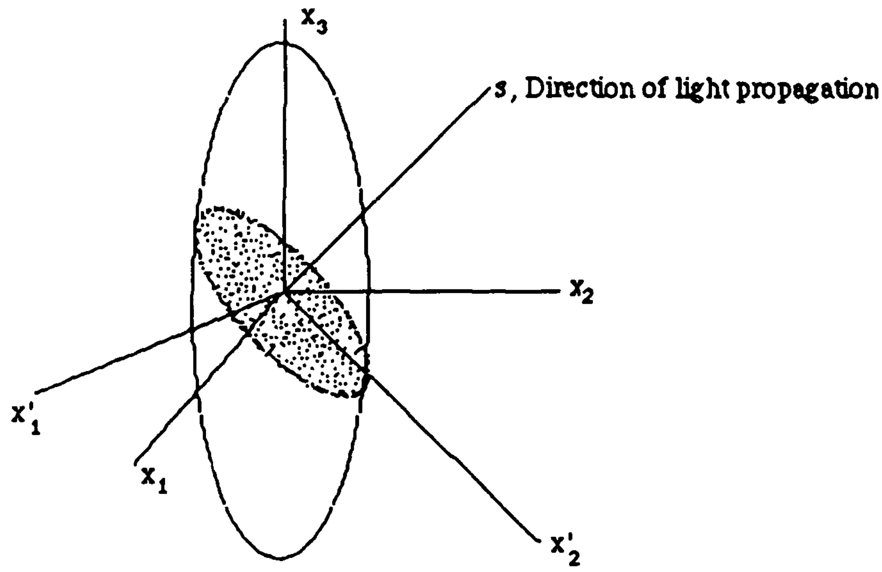

Figure 1. Fresnel ellopsoid representation of the dielectric tensor in an anisotropic material.

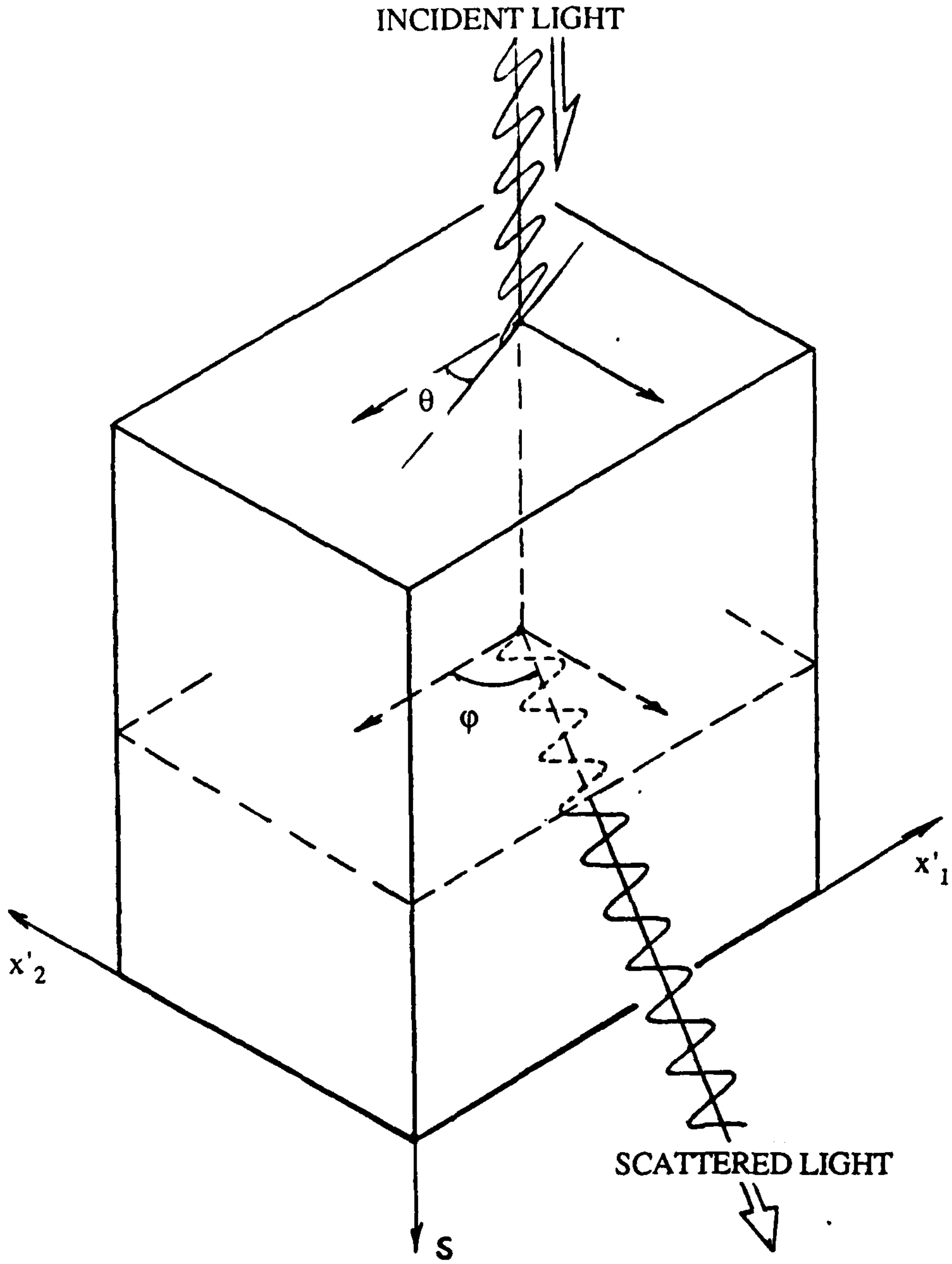

Figure 2. Geometry of light incidence and scattering from a point in the body.

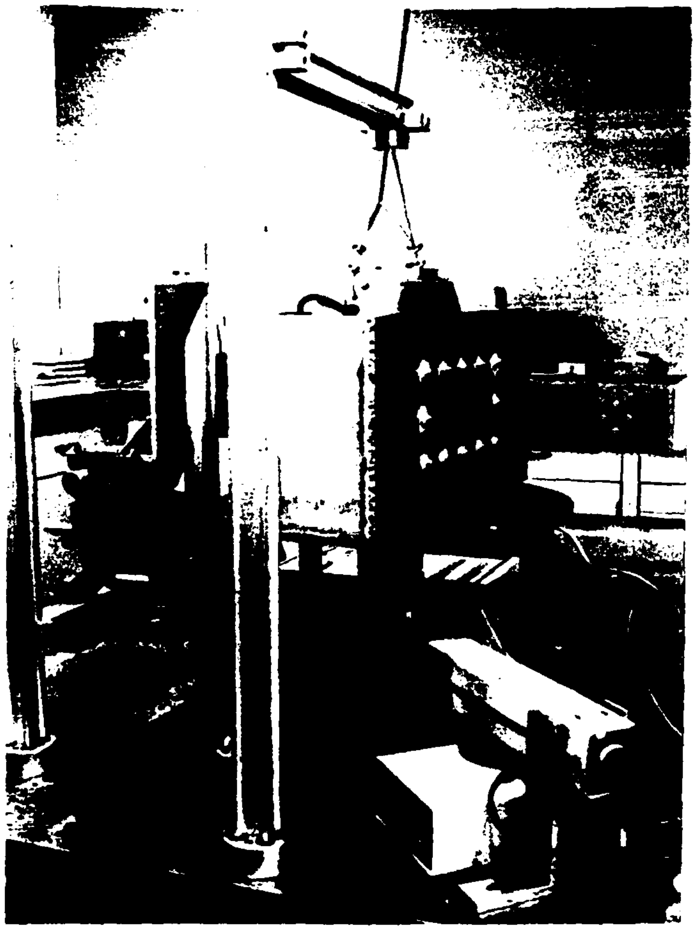

Figure 3. Scattered Light Polariscope.

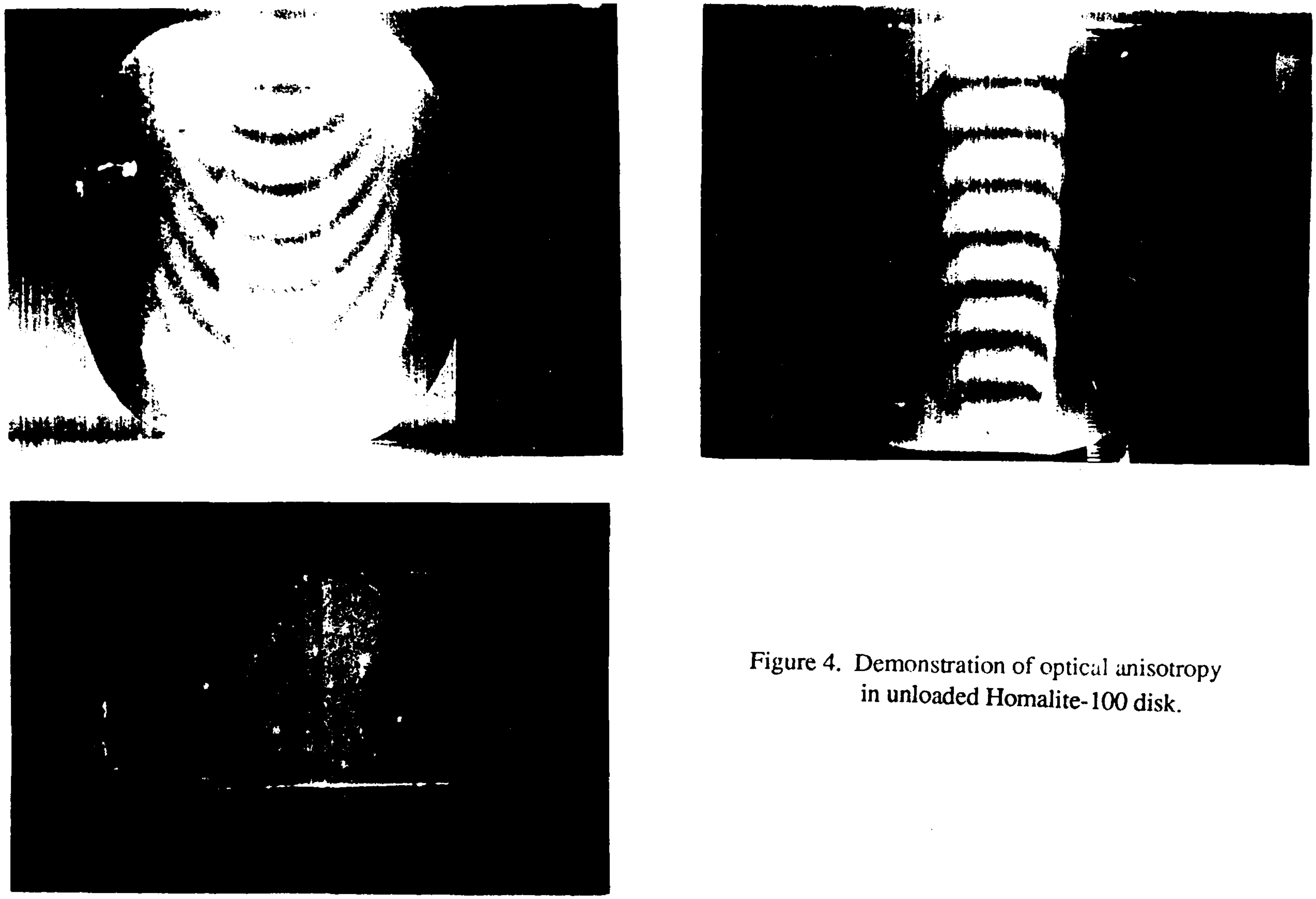

Figure 4. Demonstration of optical anisotropy
in unloaded Homalite-100 disk.

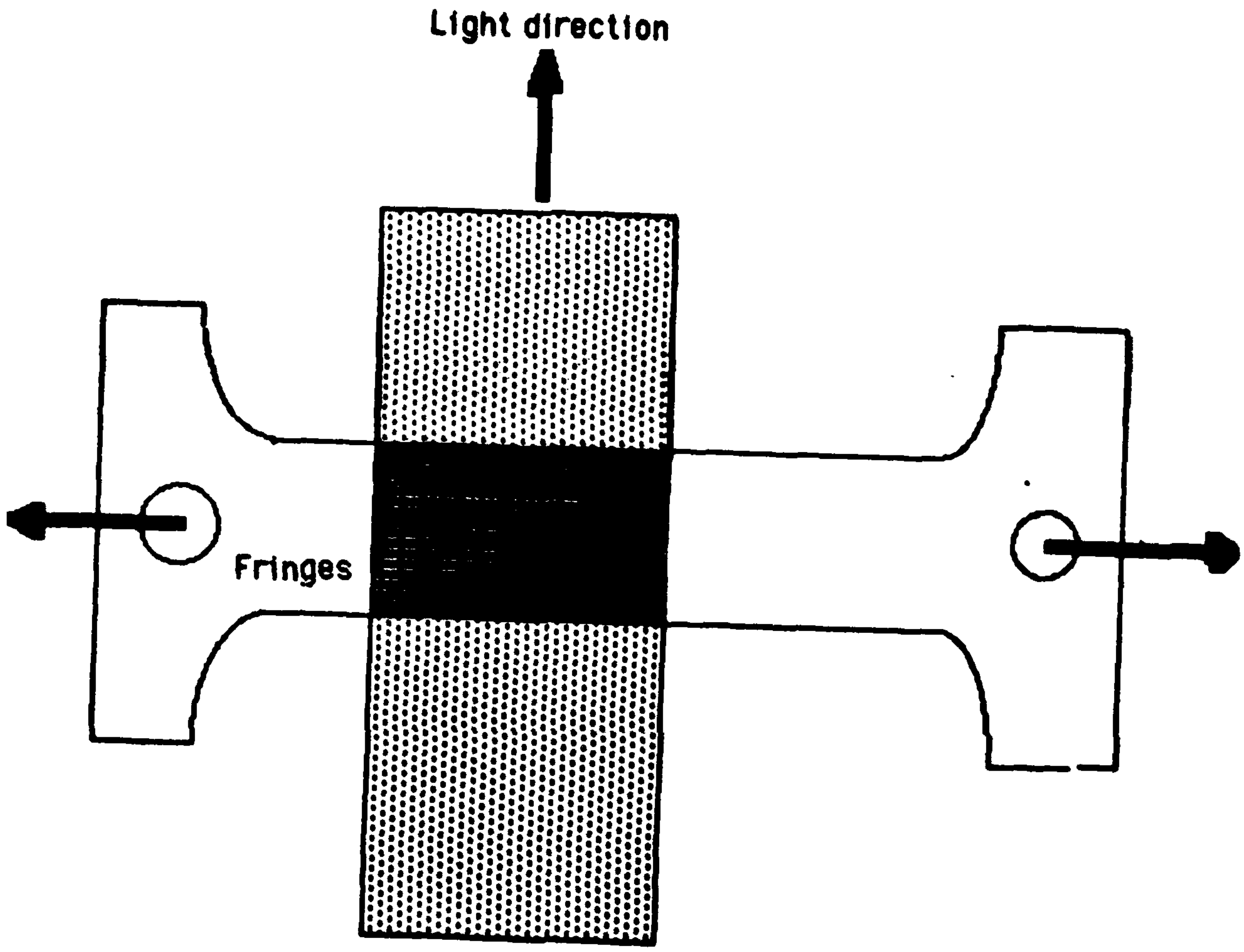

Figure 5. Scattering arrangement for a simple tension specimen.

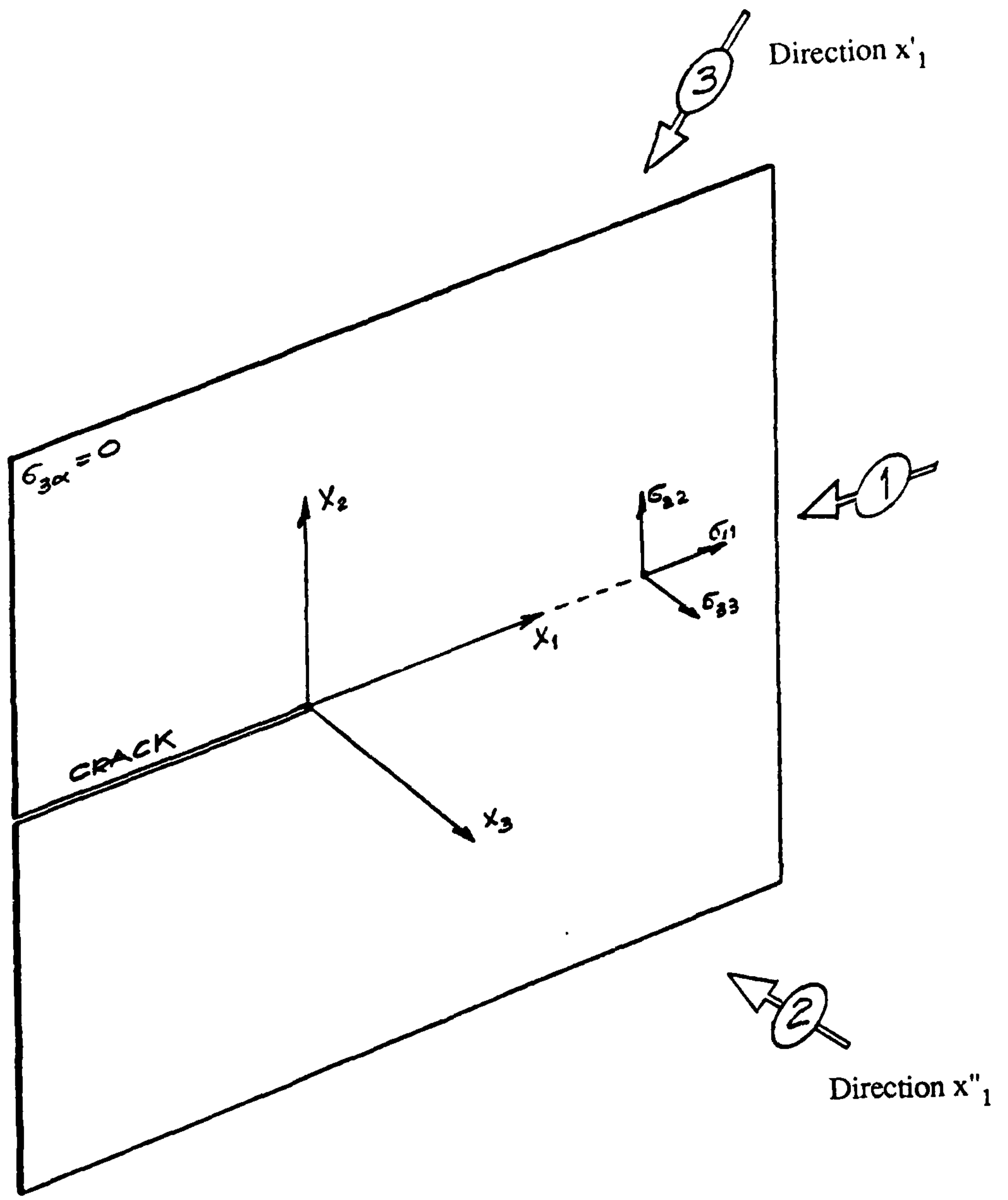

Figure 6. Geometry of scattering observations necessary for determination of all the secondary principal stress differences.

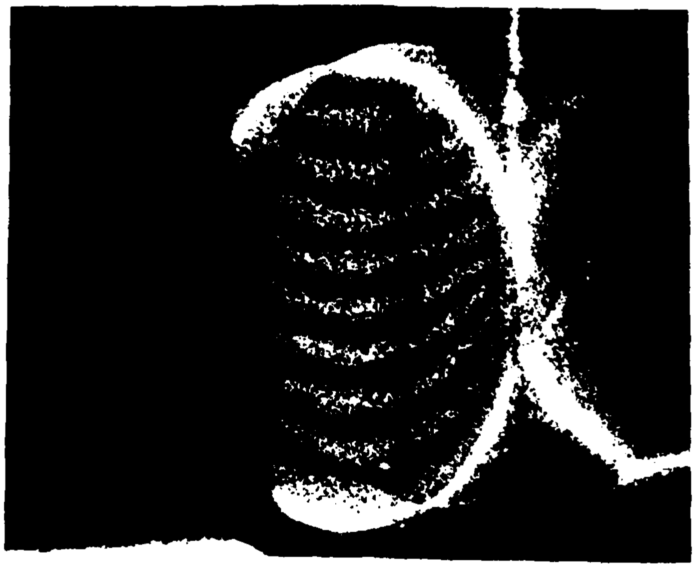

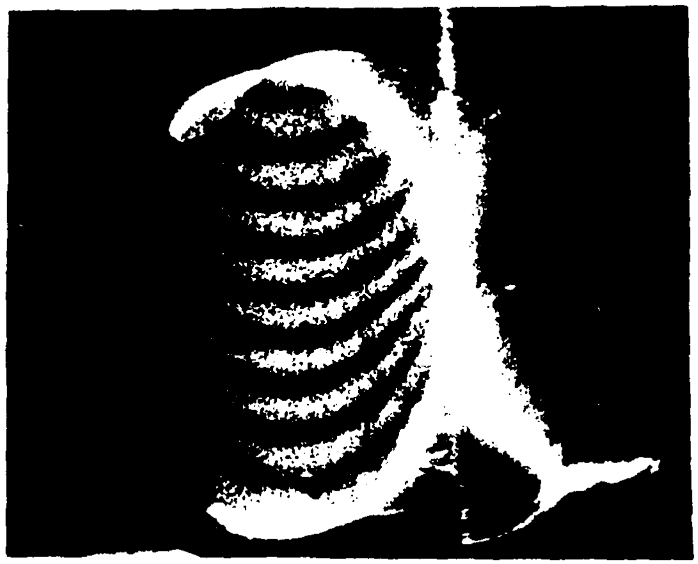

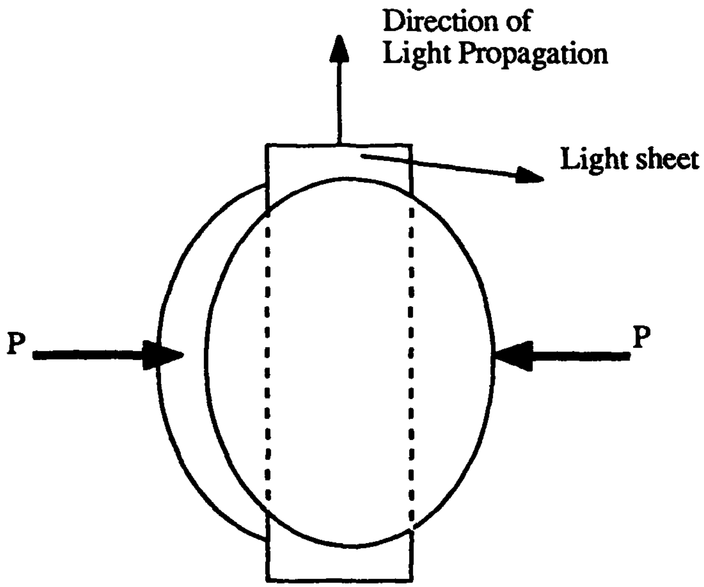

Figure 7. Disk under diametral compression. (a) Gemetry of the disk and light sheet. (b) Scattered light field in the unloaded disk (c) scattered light field in the loaded disk.

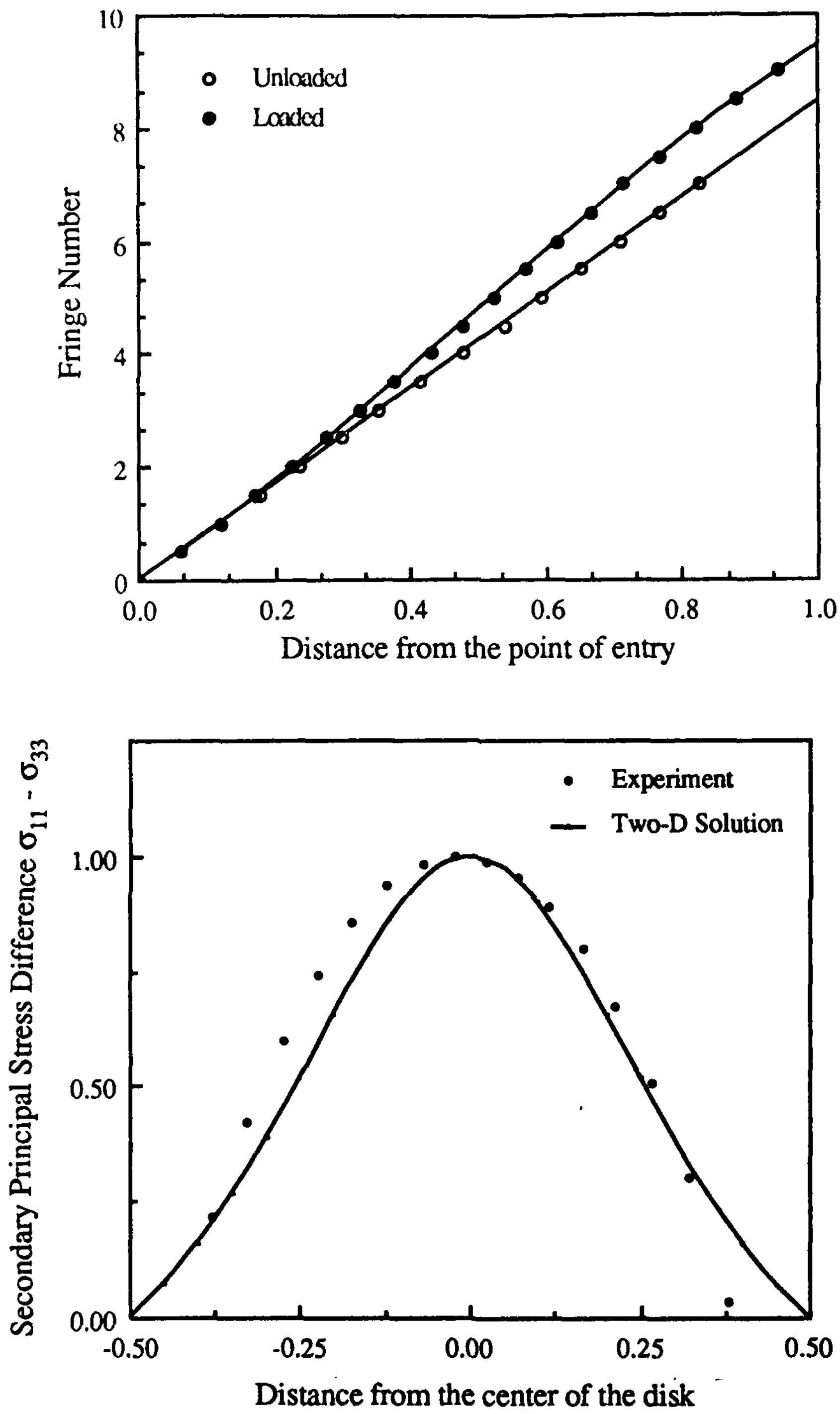

Figure 8. (a) Fringe number variation along the light path in the disk for the loaded and unloaded specimen. (b) Secondary principal stress difference calculated from the fringe patterns compared with the two dimensional elasticity solution.

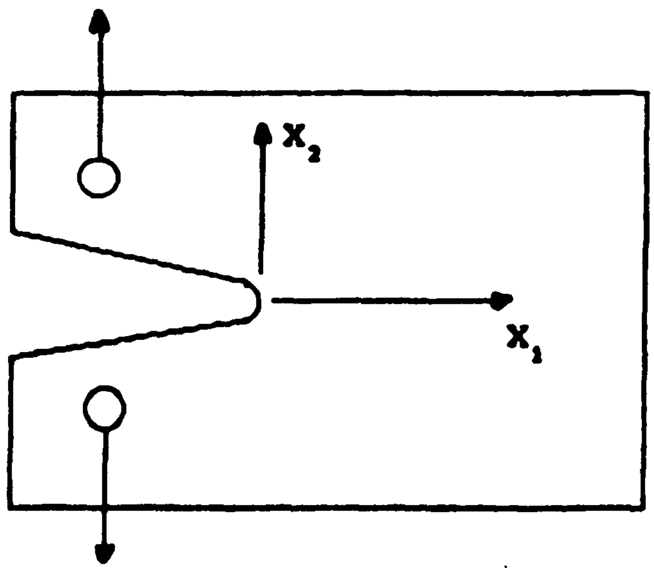

Figure 9. Geometry of the notch specimen.

Figure 10. Scattered light field in the unloaded and loaded notch specimen.

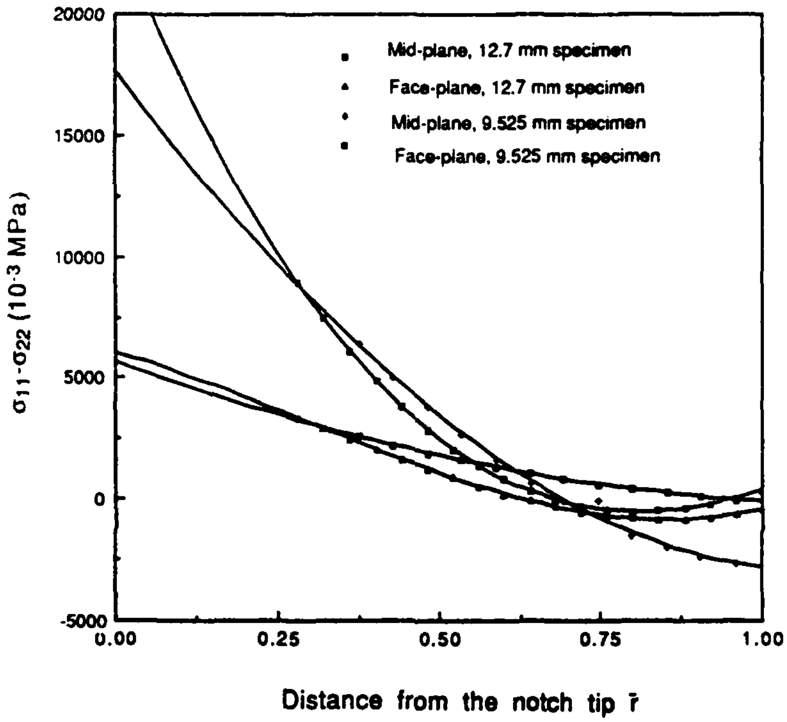

Figure 11. Variation of the secondary principal stresses in the specimen midplane and traction free surface, for two specimen thicknesses.

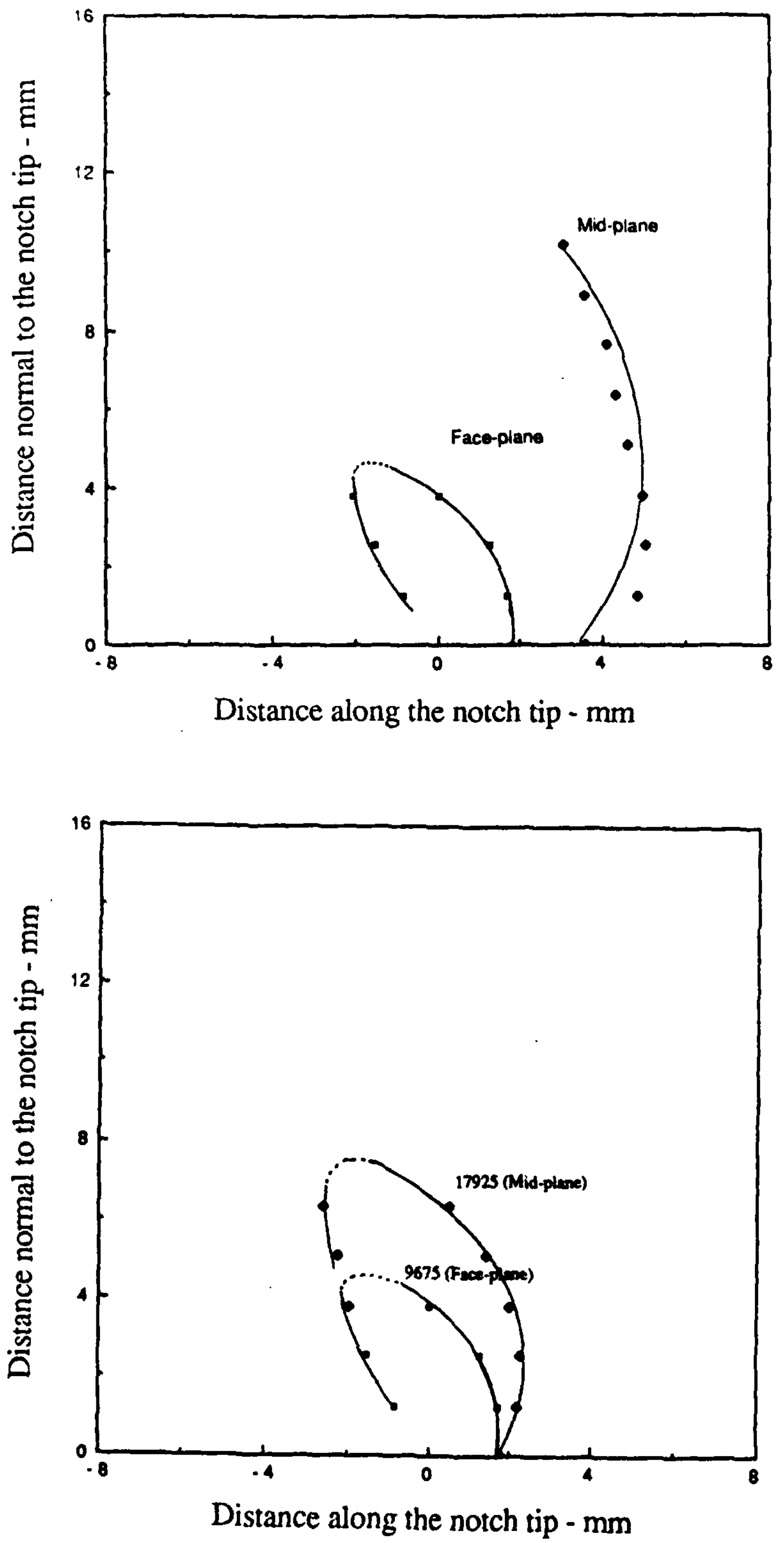

Figure 12. (a) Isochromatics on the midplane and face plane for the same value of stress difference. (b) Isochromatics that pass through the same point ahead of the notch tip (the corresponding stress differences are marked in the figure).

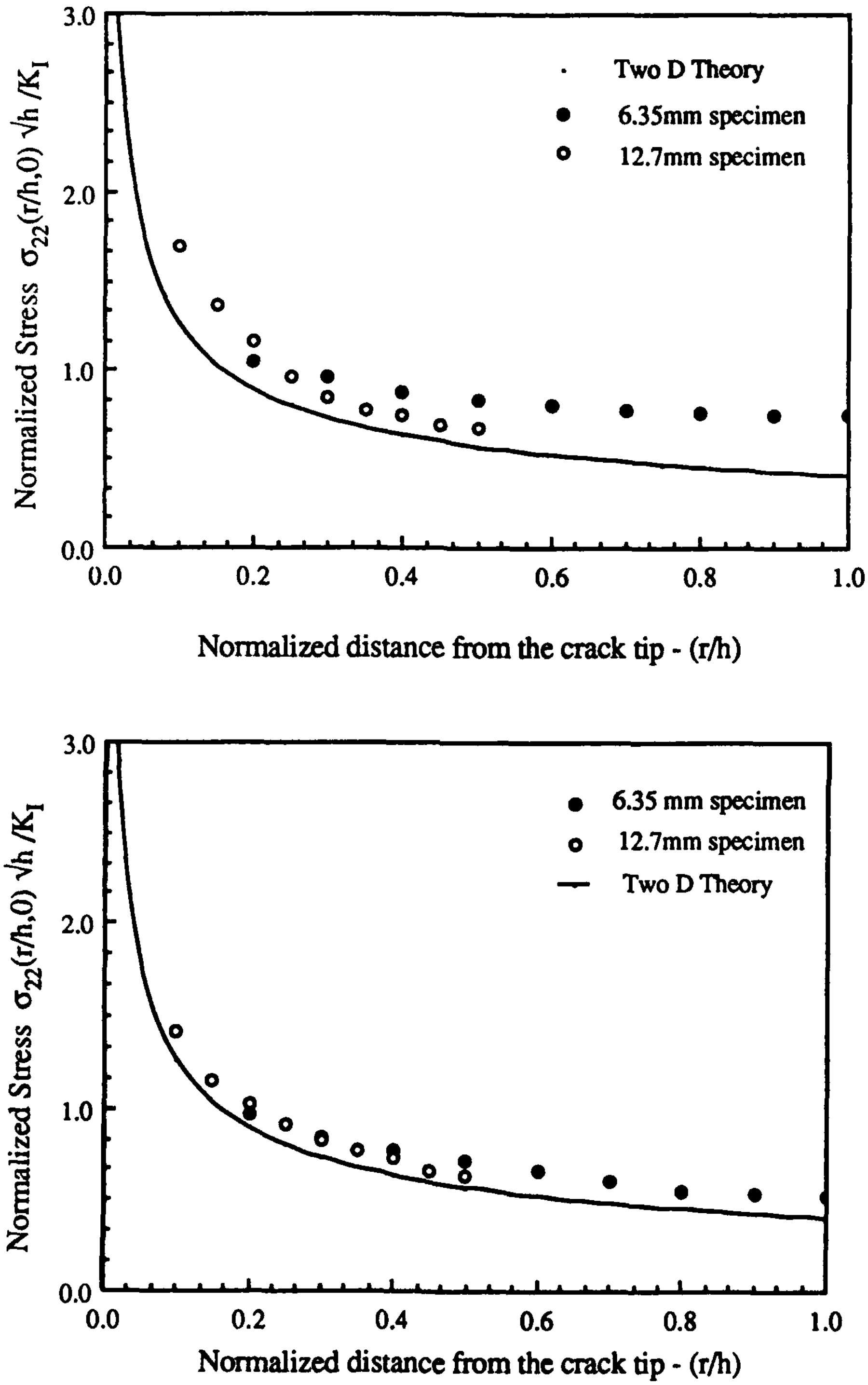

Figure 13. Variation of the normal stress ahead of the crack tip (a) in the specimen midplane and (b) in the traction free surface.

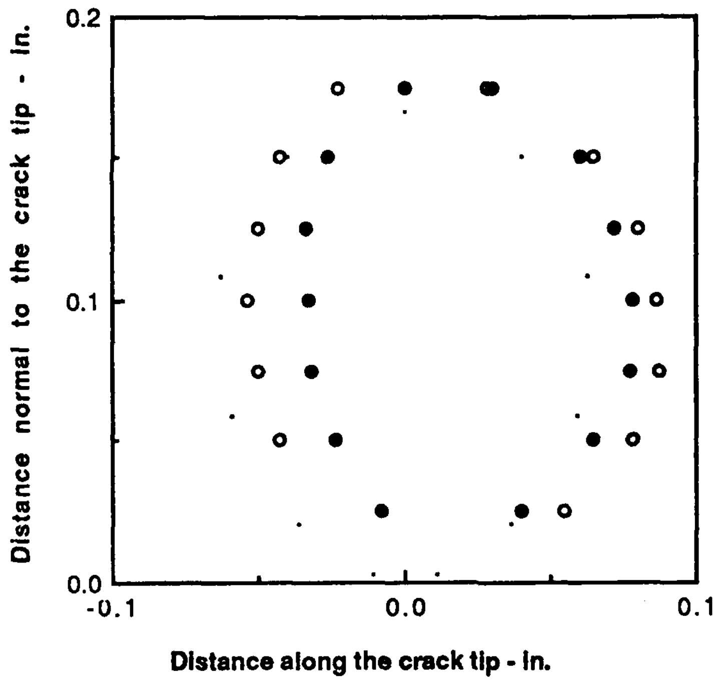

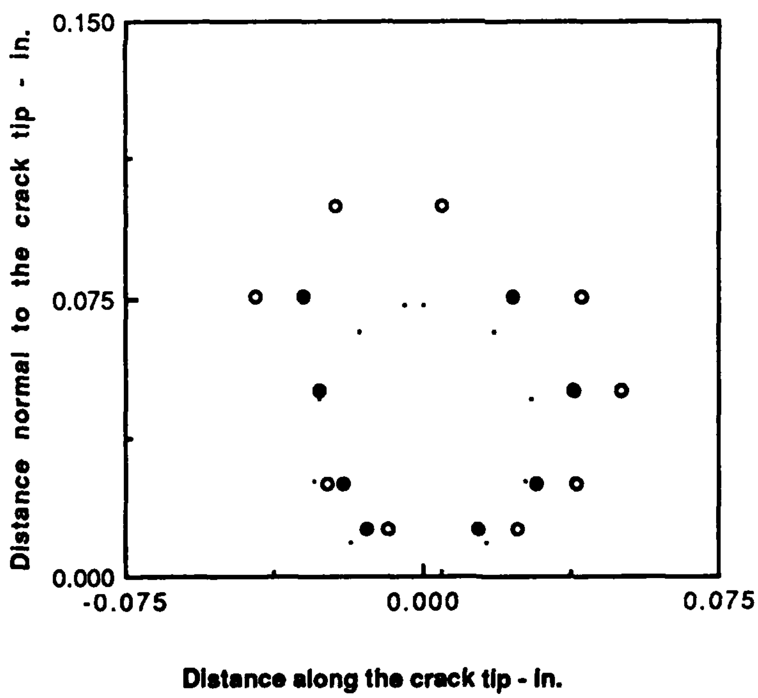

Figure 14. Isochromatics corresponding to the same value of stress difference (a) on the face plane and (b) on the specimen midplane

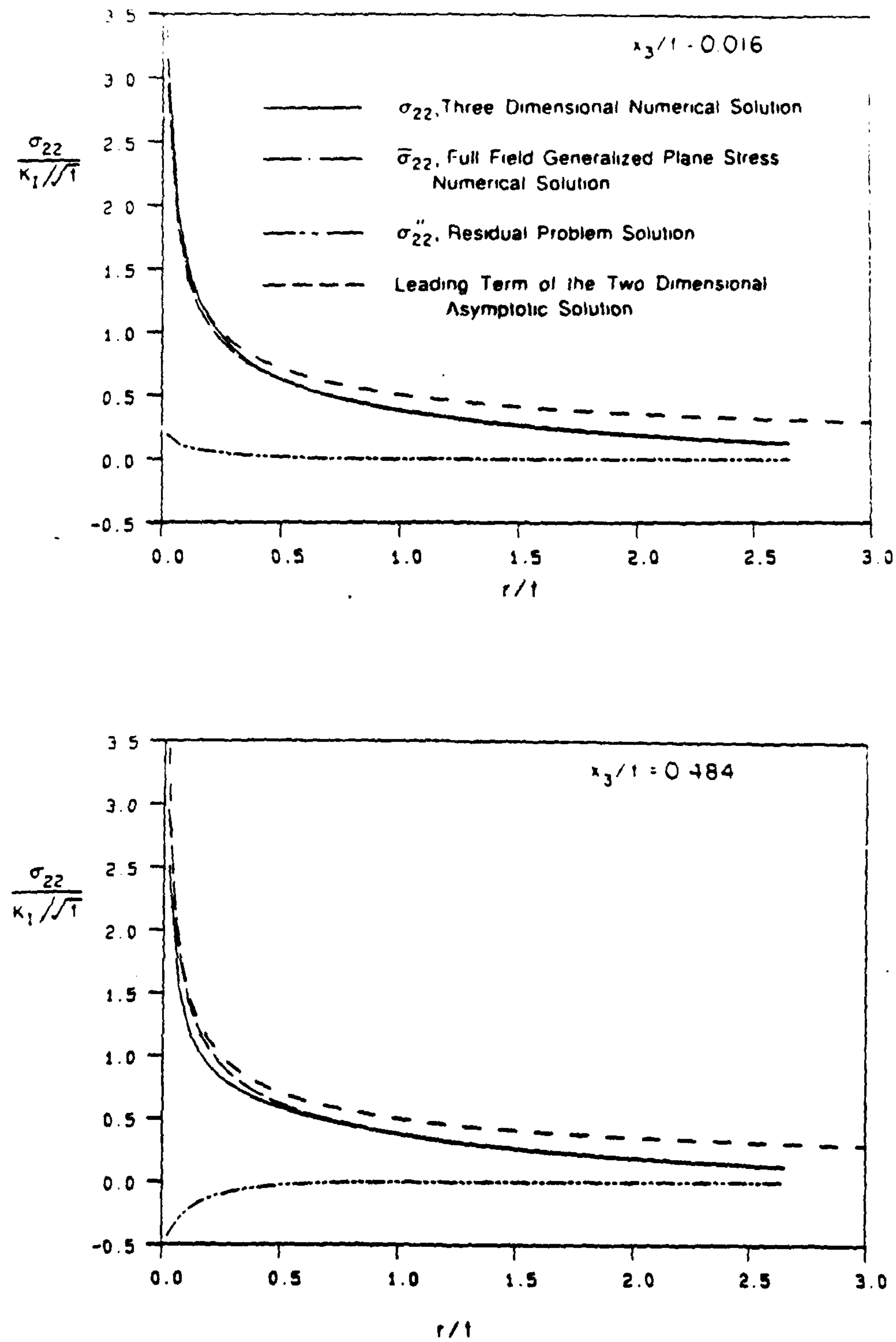

Figure 15. Variation of the normal stress ahead of the crack tip in (a) the midplane and (b) the traction free surface obtained by Parsons et al.